PAPER

On the optimum resonance of giant magnetostrictive ultrasonic transducer with capacitance-based impedance compensation

To cite this article: Huilin Zhou *et al* 2020 *Smart Mater. Struct.* **29** 105002

View the article online for updates and enhancements.

On the optimum resonance of giant magnetostrictive ultrasonic transducer with capacitance-based impedance compensation

Huilin Zhou[1] ⓘ **, Jianfu Zhang**[1,2,5] ⓘ **, Pingfa Feng**[1,2,3]**, Dingwen Yu**[1] **and Jianjian Wang**[4]

[1] Beijing Key Lab of Precision/Ultra-precision Manufacturing Equipments and Control,
Department of Mechanical Engineering, Tsinghua University, Beijing 100084 People's Republic of China
[2] State Key Laboratory of Tribology, Department of Mechanical Engineering, Tsinghua University,
Beijing 100084 People's Republic of China
[3] Division of Advanced Manufacturing, Tsinghua Shenzhen International Graduate School,
Tsinghua University, Shenzhen 518055 People's Republic of China
[4] Department of Mechanical Engineering, Northwestern University, Evanston, IL,
United States of America
[5] Author to whom any correspondence should be addressed

E-mail: zhjf@tsinghua.edu.cn

CrossMark

Abstract

Due to the large magnetostrictive coefficient, high power density and fast response speed of giant magnetostrictive materials, the giant magnetostrictive ultrasonic transducer (GMUT) becomes an increasingly popular research topic in making a high-power ultrasonic vibration. However, due to the complex energy conversion mechanism of the GMUT, the optimum resonance of the GMUT cannot be determined to utilize the ultrasonic energy to the maximum extent. To solve this problem, an equivalent circuit model of the GMUT is improved with capacitance-based impedance compensation, and the influence of the compensation capacitance on the GMUT is studied by the parameter characterization of the extreme currents and resistance points ($X = 0\ \Omega$) in the impedance circle derived from the improved model. Thus, an impedance-compensation method for determining the maximum amplitude of the GMUT is proposed to reach the optimum resonance. Experimental results show that the improved model corresponds well with the impedance circle under different compensation capacitances, and the maximum amplitude related to the optimum resonance is determined at the optimal point where the mechanical resonance and electrical resonance occur nearly simultaneously.

(Some figures may appear in colour only in the online journal)

1. Introduction

To improve machining quality, ultrasonic vibration energy has been utilized in many fields of advanced manufacturing [1–3]. Giant magnetostrictive materials (GMMs) represented by Terfenol-D [4] have the advantages of large magnetostrictive coefficient, high power density, and fast response speed. The giant magnetostrictive ultrasonic transducer (GMUT) using GMMs has become an increasingly popular research topic, and it has been utilized widely in making a high-power ultrasonic vibration, promising in terms of advanced manufacturing [5, 6]. However, due to the complex

energy conversion mechanism of the GMUT, the optimum resonance of the GMUT cannot be determined to maximize the ultrasonic-energy-utilization efficiency.

According to the previous performance tests [7, 8], Terfenol-D can effectively increase the ultrasonic amplitude and improve the ultrasonic power used in the GMUT, thus, when combined with the rotary ultrasonic machining technology, the GMUT can be applied to the processing of hard and brittle materials such as optical glass, advanced ceramics, and so on. But the temperature rising effect and load effect, which are the remaining engineering barriers to be solved in order to make GMUT a viable tool for industrial use, will lead to poor amplitude stability and also affect the resonance frequency of the system [9–11]. Thus, an efficient cooling system suitable for the GMUT is needed to be built, especially the efficient liquid cooling system which requires the components are sealed against liquid due to the coil structure in the GMUT. And an effective ultrasonic power supply with resonance frequency automatic tracking is also needed. To improve the stability of magnetostrictive system and the effectiveness of their application, many scholars have studied the temperature characteristics of GMMs and proposed temperature cooling control and resonance frequency tracking methods. Zeng *et al* [12] established a nonlinear dynamic model to explore the nonlinearity behaviors of the GMUT, demonstrating the dynamical characteristics of the system by numerical integration. Zhou *et al* [13] proposed a method of cooling GMMs by spiral tube winding. Based on the mechanism of heat generation, heat transfer, and heat dissipation, a thermodynamic model considering thermal resistance was established, and the effectiveness of the cooling method was verified by experiments. Cai *et al* [14] employed impedance analysis to identify the relevant parameters by equivalent circuit model and experiment, then explored the influence of temperature on the amplitude characteristics of the GMUT.

For frequency tracking, Zhang *et al* [15] tracked the resonance frequency of the piezoelectric system through the fuzzy logic method and binary search algorithm. Yang *et al* [16] employed the theory of fuzzy control and proportional–integral–derivative (PID) control to track frequency, and effectively compensated the static error of fuzzy control. Xu [17] used the magnetostrictive inverse effect to sense the resonance frequency of the system by driving coil or detecting coil and tracked the frequency, improving the efficiency of the transducer and effectively reducing the volume of the transducer. However, few reports explore a method of how to achieve the optimum resonance of the GMUT and the corresponding actual resonance frequency cannot be determined for high ultrasonic-energy-utilization efficiency.

This study focuses on exploring the method to realize the optimum resonance of the GMUT with capacitance-based impedance compensation. In this study, to achieve the optimum resonance of the GMUT, an equivalent circuit model of the GMUT was improved with capacitance-based impedance compensation, and the relationship between the compensation capacitance and the impedance circle of the GMUT was explored by proposing an improved impedance-compensation model with capacitance-based
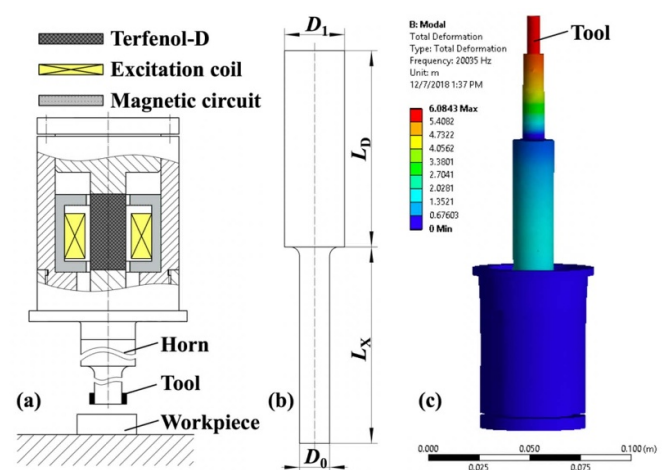
Figure 1. Schematic diagram of the GMUT: (a) Structure of the GMUT; (b) Key structural design parameters of the horn; (c) FEM simulation.

impedance compensation, which is established and identified by nonlinear fitting. To further study the resonance state of the GMUT, the discrete data point in the impedance circle was investigated, and the influence of the compensation capacitance on the GMUT was studied by the parameter characterization of the extreme currents and resistance points ($X = 0\,\Omega$) in the impedance circle derived from the improved model. Parameter identification and model verification were then carried out to put forward an impedance-compensation method for determining the maximum amplitude related to the optimum resonance of the GMUT, and the actual resonance frequency was obtained as the frequency tracking index.

2. Equivalent circuit model of the GMUT

2.1. Configuration of the GMUT

In this paper, a GMUT using Terfenol-D is designed and studied. A schematic diagram of the GMUT is shown in figure 1, in figure 1(a), the ultrasonic power supply generates a high-frequency electric signal and the excitation coil generates a high-frequency alternating magnetic field. Through the action of the magnetic circuit, the giant magnetostrictive material (Terfenol-D) generates longitudinal ultrasonic vibration along the axial direction in the GMUT. The vibration is then transmitted and amplified through the horn so that the tool can remove material of the workpiece.

Figure 1(b) provides the key structural design parameters of the horn. To achieve the maximum amplitude at the output end of the horn, according to the vibration transmission principle of a longitudinal wave, one-dimensional longitudinal vibration occurring in the horn is supposed. The input end of the horn, i.e. the connection surface with the transducer, is designed as the peak/trough position, and the step surface connected at the large and small ends of the horn is considered as the nodal surface to reduce the energy loss of reflected wave. Therefore, considering the rationality of the length design, the total length of the horn is selected as half wavelength and $L_D = L_X = \lambda/4$.

Table 1. Key structural design parameters of the horn.

Parameter	Unit	Design value
Length of the large end L_D	mm	63.095
Length of the small end L_X	mm	63.095
Diameter of the small end D_0	mm	10
Diameter of the large end D_1	mm	20
Design resonance frequency (initial value)	kHz	20
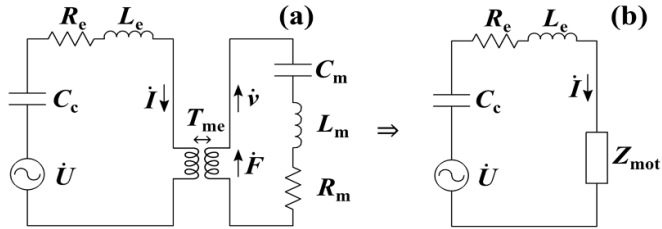
Figure 2. Coupling equivalent process of the electric circuit of the GMUT: (a) Electromechanical equivalent circuit; (b) Coupling equivalent circuit [18].

Because the longitudinal wave velocity satisfies $c = \sqrt{E/\rho}$, and $c = f\lambda$, where E and ρ represent Young's modulus and density of the horn, f represents the frequency, and λ represents the wavelength. Therefore, according to the parameters given by 45# steel material and the design resonance frequency of 20 kHz, the calculation results are $c = 5047.6 \, \text{m s}^{-1}$, $\lambda = 252.38$ mm, and $L_D = L_X = 63.095$ mm.

Table 1 provides the key structural design parameters of the horn in detail. According to the amplitude magnification coefficient, the reasonable values of the-small-end diameter D_0 and the-large-end diameter D_1 can be determined. Usually, the actual resonance frequency of the GMUT changes due to the existence of structures such as tool, shape of horn, and joint surface. A FEM simulation is needed to make the longitudinal-mode frequency close to the design resonance frequency, which may require changing the key structural design parameters of the horn, as shown in figure 1(c). It is therefore necessary to further explore the optimal output state of the amplitude for the GMUT.

2.2. Equivalent circuit model of the GMUT

As noted in the literatures [18–20], the equivalent circuit model has been used to study the vibration performance of the GMUT. However, the influence of the impedance compensation on the resonance of the GMUT cannot be studied by the model, and the optimum resonance cannot be determined. Thus, an improved impedance-compensation model with capacitance-based impedance compensation is proposed based on the equivalent circuit model. Figure 2 shows the coupling equivalent process of the electric circuit of the GMUT, in which figure 2(a) illustrates the electromechanical equivalent circuit and figure 2(b) is the coupling equivalent circuit.

In figure 2, $\dot{U}$ and $\dot{I}$ represent the voltage and current, respectively, $\dot{F}$ and $\dot{v}$ represent the driving force and speed,

respectively, and the electric impedance of the equivalent circuit includes electric resistance R_e, electric inductance L_e, and compensation capacitance C_c. The mechanical impedance of the equivalent circuit includes the mechanical resistance R_m, the mechanical inductance L_m, and the mechanical capacitance C_m. The coupling parameters include the electromechanical conversion coefficient T_{me} and the coupling dynamic impedance Z_{mot}.

The equivalent circuit model of the GMUT can be expressed in the form of impedance circle, however, the relationship between the compensation capacitance and the impedance circle has not been not explored in the equivalent circuit model. To effectively explore the relationship, it is necessary to further analyze and solve the equivalent circuit of the GMUT, and establish an improved impedance-compensation model. According to the existing literature [19, 20], the key parameters in the coupling equivalent circuit process can be expressed as:

$$\begin{cases} Z_m = R_m + j\omega L_m + \dfrac{1}{j\omega C_m} \\[2mm] Z_{mot} = -\dfrac{T_{em}T_{me}}{Z_m} \\[2mm] T_{em} = -T_{me} \end{cases} \tag{1}$$

where ω is the circular frequency in the impedance circle and the loss in the process of energy conversion is ignored. The coupling dynamic impedance Z_{mot} is given by:

$$Z_{mot} = R_{mot} + jX_{mot}. \tag{2}$$

Therefore, it can be obtained from equations (1) and (2) that:

$$\begin{cases} R_{mot} = \dfrac{T_{me}^2 R_m}{R_m^2 + \left(\omega L_m - \dfrac{1}{\omega C_m}\right)^2} \\[4mm] X_{mot} = -\dfrac{T_{me}^2 \left(\omega L_m - \dfrac{1}{\omega C_m}\right)}{R_m^2 + \left(\omega L_m - \dfrac{1}{\omega C_m}\right)^2} \end{cases}. \tag{3}$$

Equation (3) reduces to the common expression:

$$\left(R_{mot} - \dfrac{T_{me}^2}{2R_m}\right)^2 + X_{mot}^2 = \left(\dfrac{T_{me}^2}{2R_m}\right)^2 \tag{4}$$

thus the total impedance of the GMUT can be expressed as:

$$Z = R + jX \tag{5}$$

where Z is the total impedance, R is the resistance, and X is the reactance.

$$\begin{cases} R = R_e + R_{mot} \\[2mm] jX = jX_{mot} + j\omega L_e + \dfrac{1}{j\omega C_c} \end{cases}, \tag{6}$$

Further substituting equation (6) into equation (4), the equivalent circuit model of the GMUT can be derived as follows:

$$\left(R - \dfrac{T_{me}^2}{2R_m} - R_e\right)^2 + \left(X - \omega L_e + \dfrac{1}{\omega C_c}\right)^2 = \left(\dfrac{T_{me}^2}{2R_m}\right)^2. \tag{7}$$

To simplify the equivalent circuit model of the GMUT, equation (8) is given as:

$$\begin{cases} r = \dfrac{T_{me}^2}{2R_m} \\[2mm] A = \dfrac{T_{me}^2}{2R_m} + R_e \\[2mm] B = \omega L_e - \dfrac{1}{\omega C_c} \end{cases} \qquad (8)$$

It can be seen that r and A are independent of the circular frequency ω and the compensation capacitance C_c, however, ω and C_c may have an uncertain effect on B. Substituting equation (8) into equation (7) obtains:

$$(R - A)^2 + (X - B)^2 = r^2 \qquad (9)$$

where A and B represent the abscissa and ordinate of the impedance circle center, respectively, and r is the radius of the impedance circle.

2.3. Improved impedance-compensation model

To obtain the improved impedance-compensation model, the key parameters of the model are mathematically studied using equation (8). To calculate the effective ordinate B of the impedance circle center, the model must be transformed further. Thus, zero compensation capacitance is defined as C_0 by solving equation (10):

$$\omega_n L_e = \frac{1}{\omega_n C_0} \qquad (10)$$

where ω_n is the mechanical resonance circular frequency of the GMUT, $B = 0$ while $C_c = C_0$, and the system will reach the mechanical resonance ($\omega = \omega_n$). Thus, C_c can be expressed as:

$$C_c = C_0 + \Delta C \qquad (11)$$

where ΔC is the offset of the compensation capacitance. It should be noted that the units of C_c, C_0, and ΔC in this study are nF. Substituting equation (11) into equation (8), and splitting B, provides:

$$\begin{aligned} B &= \omega L_e - \frac{1}{\omega C_c} = \omega L_e - \frac{1}{\omega(C_0 + \Delta C)} \\ &= \omega L_e - \frac{1}{\omega C_0} + \frac{\Delta C}{\omega C_0(C_0 + \Delta C)}. \end{aligned} \qquad (12)$$

Considering the relationship between the circular frequency ω and frequency f in equation (13), i.e.

$$\omega = 2\pi f, \qquad (13)$$

an effective cut-off frequency interval near the mechanical resonance frequency f_n in the impedance circle of the GMUT is assumed where the influence of the frequency change on the

first two items of B within the interval can be ignored. This means:

$$\omega L_e - \frac{1}{\omega C_0} \approx \omega_n L_e - \frac{1}{\omega_n C_0} = 0. \qquad (14)$$

The effective cut-off frequency interval is obtained and verified below. Substituting equation (14) into equation (12) yields:

$$B = \omega L_e - \frac{1}{\omega C_0} + \frac{\Delta C}{\omega C_0(C_0 + \Delta C)} = \frac{\Delta C}{\omega C_0(C_0 + \Delta C)} \qquad (15)$$

by substituting equation (11) into equation (15), B can then be rewritten as:

$$\begin{aligned} B &= \frac{\Delta C}{\omega C_0(C_0 + \Delta C)} = \frac{C_c - C_0}{\omega C_0 C_c} \\ &= \frac{1}{\omega}\left(\frac{1}{C_0} - \frac{1}{C_c}\right) \approx \frac{1}{\overline{\omega}}\left(\frac{1}{C_0} - \frac{1}{C_c}\right) \end{aligned} \qquad (16)$$

where ω is considered as the average constant $\overline{\omega}$, representing the fitting circular frequency. Substituting equation (16) into equation (9), the improved impedance-compensation model can be established as:

$$(R - A)^2 + \left[X - \frac{1}{\overline{\omega}}\left(\frac{1}{C_0} - \frac{1}{C_c}\right)\right]^2 = r^2 \qquad (17)$$

3. Parameter characterization

3.1. Frequency angle α of the impedance circle

For a real GMUT device, the discrete data points and frequencies obtained cannot directly connect with the compensation capacitances. To study the impedance-compensation characteristics including the extreme currents (minimum current and maximum current) and resistance points ($X = 0\ \Omega$) in the impedance circle, parameter characterization of the frequency angle α of the impedance circle is proposed to establish the relationship between the frequency of each discrete data point and the point's position in the impedance circle.

The value distribution of the frequency angle α in the impedance circle is shown in figure 3, α represents the angle composed of the line from the center of the impedance circle to the discrete point and the abscissa, with the unit of $°$. The α in first and third quadrants represents $\alpha > 0°$, and the α in second and fourth quadrants represents $\alpha < 0°$, using $\alpha = 0°$ for the abscissa. Thus, two kinds of special frequency angles are further defined to illustrate the impedance-compensation characteristics according to the improved impedance-compensation model.

3.2. Extreme frequency angle α_{ext} of the impedance circle

To explore the relationship between the compensation capacitance C_c and extreme currents in the impedance circle, the extreme frequency angle α_{ext} of the impedance circle is proposed, which consists of the frequency angles with the
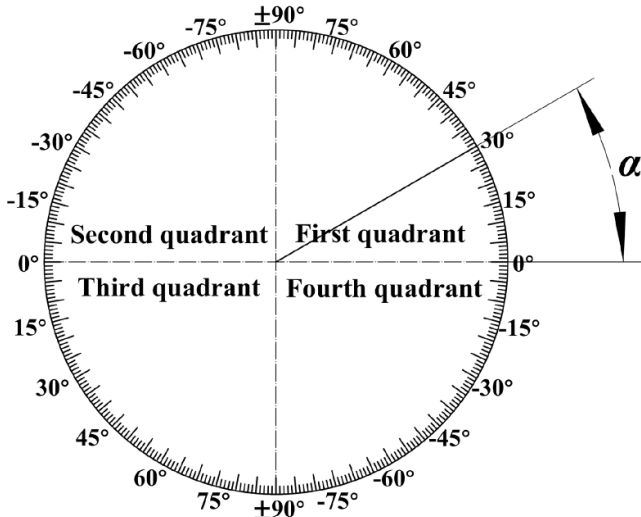
Figure 3. Value distribution of the frequency angle α in the impedance circle.

Figure 4. Geometric relationship between the improved impedance-compensation model and the extreme frequency angles of the impedance circle.

maximum value and minimum value of the total impedance mode in the impedance circle represented by α_{ext1} and α_{ext2}, respectively. The geometric relationship between the improved impedance-compensation model and the extreme frequency angles α_{ext1} and α_{ext2} of the impedance circle is then established, as shown in figure 4.

In figure 4, the circles O_0, O_1, and O_2 represent the impedance circles when $C_c > C_0$, $C_c = C_0$, and $C_c < C_0$, respectively. For each kind of impedance circle, there are a maximum $|Z(C_c)|_{\max}$ and minimum value $|Z(C_c)|_{\min}$ of the total impedance mode given by:

$$
\begin{cases}
|Z(C_c)|_{\min} = \overline{OO_5} = \sqrt{A^2 + B^2} - r \\
\qquad = \sqrt{\left(\dfrac{T_{me}^2}{2R_m} + R_e\right)^2 + \left[\dfrac{1}{\omega}\left(\dfrac{1}{C_0} - \dfrac{1}{C_c}\right)\right]^2} - \dfrac{T_{me}^2}{2R_m} \\
|Z(C_c)|_{\min} = \overline{OO_6} = \sqrt{A^2 + B^2} - r \\
\qquad = \sqrt{\left(\dfrac{T_{me}^2}{2R_m} + R_e\right)^2 + \left[\dfrac{1}{\omega}\left(\dfrac{1}{C_0} - \dfrac{1}{C_c}\right)\right]^2} + \dfrac{T_{me}^2}{2R_m}
\end{cases}
\tag{18}
$$

In combination with figures 3 and 4, it can be seen that in any case, this will provide:

$$
\alpha_{ext1}(C_c) = \alpha_{ext2}(C_c). \tag{19}
$$

Therefore, $\alpha_{\text{ext}}(C_c)$ can be expressed as:

$$
\alpha_{ext}(C_c) = \arctan\left(\frac{B}{A}\right) = \arctan\left[\frac{\frac{1}{\omega}\left(\frac{1}{C_0} - \frac{1}{C_c}\right)}{\frac{T_{me}^2}{2R_m} + R_e}\right] \tag{20}
$$

It can be seen from equation (20) that when $C_c = C_0$, there are:

$$
\alpha_{ext}(C_c) = 0°. \tag{21}
$$

Simultaneously, the maximum value $|Z(C_c)|_{\max}$ and the minimum value $|Z(C_c)|_{\min}$ of the total impedance mode in the impedance circle reach the minimum value $|Z(C_0)|_{\max\,|\,\min}$ and $|Z(C_0)|_{\min\,|\,\min}$, respectively.

3.3. Resistance frequency angles α_{res1} and α_{res2} of the impedance circle

The effective resistance points ($X = 0\ \Omega$) in the impedance circle are also studied to further explore the impedance-compensation characteristics. The geometric relationship between the improved impedance-compensation model and the resistance frequency angles of the impedance circle is shown in figure 5, the intersection points of the impedance circle and abscissa are defined as the resistance point, including the first and the second resistance points, and the second resistance point is the one with higher frequency (points O_2 and O_4). As the frequency difference between two resistance points is large when $C_c < C_0$, and the frequency of the second resistance point will be far away from the mechanical resonance frequency of the GMUT as C_c decreases, the improved impedance-compensation model is discussed for when $C_c \geq C_0$.

The $\alpha_{\text{res1}}(C_c)$ and $\alpha_{\text{res2}}(C_c)$ respectively represent the resistance frequency angles of the impedance circle, which are
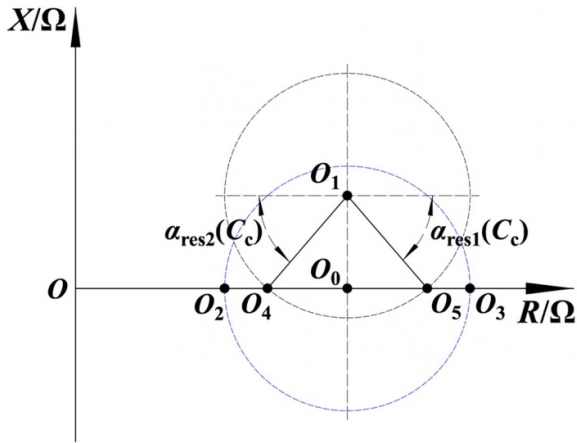
Figure 5. Geometric relationship between the improved impedance-compensation model and the resistance frequency angles of the impedance circle.

the frequency angles of the impedance circle showing the pure resistance characteristic. In combination with figures 3 and 5, they can be defined as:

$$\alpha_{res1}(C_c) = -\alpha_{res2}(C_c), \; \alpha_{res1}(C_c) \leqslant 0, \; C_c \geqslant C_0 \quad (22)$$

while $\alpha_{res1}(C_c)$ can be given by:

$$\alpha_{res1}(C_c) = -\arcsin(\frac{\overline{O_0O_1}}{\overline{O_1O_5}}) = -\arcsin(\frac{B}{r})$$

$$= -\arcsin\left[\frac{\frac{1}{\omega}\left(\frac{1}{C_0} - \frac{1}{C_c}\right)}{\frac{T_{me}^2}{2R_m}}\right] \quad (23)$$

4. Experiments and discussion

To explore the method for determining the maximum amplitude of the GMUT, the current variation and the in-phase point of the voltage and current in the impedance circle must be obtained and investigated. Since the GMUT is an electromagnetic-mechanical coupling system, the electric energy input to the GMUT makes Terfenol-D produce magnetostriction through the electromagnetic field, and the acoustic wave energy in the vibration system appears as mechanical energy of vibration through the amplification of the horn. From a physical point of view, the actual resonance frequency of the GMUT is not only related to the resonance frequency of the mechanical structure (i.e. the mechanical resonance frequency f_n) but also related to the energy input to the system.

From the perspective of energy conversion, the energy conversion efficiency of the GMUT can be expressed as the product of electrical energy conversion efficiency and mechanical energy conversion efficiency. For the electrical energy conversion efficiency, when the voltage and current are in phase (electrical resonance, $X = 0 \; \Omega$), all the input energy is converted into useful work acting on the Terfenol-D, and the electrical energy conversion efficiency reaches the maximum. For the mechanical energy conversion efficiency, when the vibration frequency is at the mechanical resonance frequency,

the mechanical structure resonates, and the mechanical energy conversion efficiency reaches the maximum. Thus, the energy conversion efficiency of the GMUT reaches its maximum only when the electrical resonance frequency is consistent with the mechanical resonance frequency. However, the useful work input to the GMUT cannot reach the maximum at the maximum energy conversion efficiency, and the maximum amplitude related to the optimum resonance cannot be realized due to the impedance-compensation characteristics of the GMUT.

Thus, it is, therefore, necessary to study impedance-compensation characteristics in the impedance circle, including the extreme currents and the resistance points. This allows for further exploration of a method to determine the actual resonance frequency.

4.1. Experimental setup

As shown in figure 6, the impedance analyzer was used to collect the frequency-sweeping information of the resistance and reactance of each discrete data point in the impedance circle of the GMUT, the frequency-sweeping range was set to 19 500 Hz-21 000 Hz, with a step of 1 Hz. The compensation capacitance was utilized for compensating the circuit with the smallest adjustable amount of 1 nF. The ultrasonic power supply excited the GMUT with electrical signals at constant voltages and the laser displacement sensor was used to measure the amplitude at the end of the horn of the GMUT using 392 kHz-sampling frequency. The oscilloscope was then employed to display the real-time current signal induced by the current sensor, the power meter collected and calculated the current. In figure 6(a), the computer outputted the control signal to control the impedance analyzer (S1) or the ultrasonic power supply and laser displacement sensor (S2), and each experiment is conducted in a short time to avoid the temperature rising error caused by the eddy current effect in the GMUT. The experimental setup is shown in figure 6(b).

4.2. Parameter identification and model validation

4.2.1. Effective cut-off frequency interval. To determine the effective cut-off frequency interval near the mechanical resonance frequency in the impedance circle of the GMUT, appropriate discrete data points in the impedance circle need to be selected. Under the same compensation capacitance, each discrete data point in the impedance circle represents the impedance-compensation characteristics under different excitation frequencies, i.e. each point in the impedance circle corresponds to different B, so when the distribution of the discrete data points is too dense (resulting from large frequency variation), the variation of the frequency will cause the shape of the impedance circle deviate from the circle. Thus, using discrete data points with too dense distribution as fitting data points can cause fitting distortion of the improved impedance-compensation model.

To reduce the influence of the frequency on B and identify the effective model of the impedance circle, the frequency-distance impedance mode d_Z is defined, representing the size
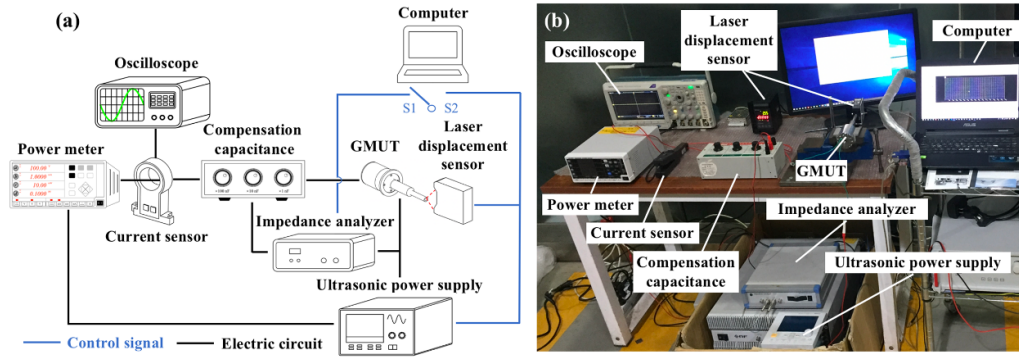
Figure 6. Illustration of the experimental setup: (a) Schematic diagram of experimental device; (b) Experimental setup.
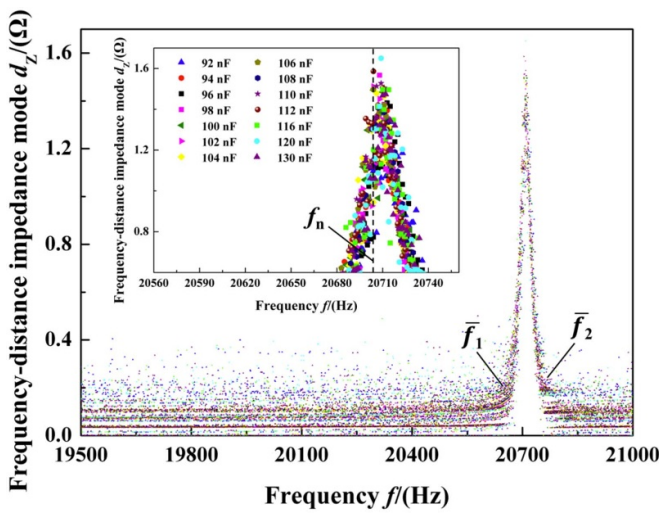
Figure 7. Distribution of the frequency-distance impedance mode d_Z of the discrete data points under different compensation capacitances.

of the impedance mode between two discrete data points in the impedance circle with one unit frequency difference, that is:

$$d_Z = \sqrt{(R_{f+1Hz} - R_f)^2 + (X_{f+1Hz} - X_f)^2} \qquad (24)$$

where R_f and X_f respectively represent the resistance and reactance at the frequency f, and $R_{f+1\ Hz}$ and $X_{f+1\ Hz}$ represent the resistance and reactance at the frequency $f + 1$ Hz.

To determine the effective cut-off frequency interval, d_Z needs to be calculated. Thus, the impedance analyzer was used to collect the resistance and reactance of the GMUT under different compensation capacitances by frequency sweeping, and the results for d_Z according to the statistics of the discrete data points in the impedance circle is shown in figure 7.

In figure 7, the d_Z under different compensation capacitances displays a mutation in a certain frequency range, and the average values of the effective cut-off frequencies of d_Z for the mutation under different compensation capacitances are defined as $\overline{f_1}$, $\overline{f_2}$, respectively, which are expressed as $\overline{f_1} = 20\,657$ Hz, $\overline{f_2} = 20\,772$ Hz. In the interval $[\overline{f_1}, \overline{f_2}]$, distribution of the d_Z appears a sudden change (d_Z spike) when the frequency is near the mechanical resonance frequency f_n, the

mechanical resonance frequency is determined according to the existing literature [19], i.e. $f_n = 20\,704$ Hz in this study. Therefore, the rationality of a design mechanical resonance frequency f_n of a GMUT in FEM simulation can be verified by the frequency of the d_Z spike in the effective cut-off frequency interval. With an increase in f, d_Z first increases and then decreases, and the distance between the discrete data points in the impedance circle first increases and then decreases. That is to say, most of the discrete data points in the circle appear in the interval $[\overline{f_1}, \overline{f_2}]$.

The frequency difference $\Delta\bar{f}$ of the interval $[\overline{f_1}, \overline{f_2}]$ in the impedance circle of the GMUT is:

$$\Delta\bar{f} = \overline{f_2} - \overline{f_1} = 115\ Hz \qquad (25)$$

where $\Delta\bar{f}$ is far smaller than the mechanical resonance frequency f_n of the GMUT. It is, therefore, assumed that the interval $[\overline{f_1}, \overline{f_2}]$ is the effective cut-off frequency interval, which means that the influence of the frequency change on B within the effective cut-off frequency interval is ignored.

4.2.2. Abscissa A of the impedance circle center and radius r of the impedance circle. According to the interval $[\overline{f_1}, \overline{f_2}]$, the average number of the effective discrete data points under every compensation capacitance was selected, and the least square method was used to fit the effective discrete data points in each impedance circle by MATLAB.

The relation diagram of the abscissa A, ordinate B of the fitted circle center and the radius r of the fitted circle versus the compensation capacitance C_c of the GMUT is provided below in figures 8 and 9.

According to equation (8) and figures 8 and 9, it can be seen that r and A are independent of the frequency f and the compensation capacitance C_c, and their values are basically unchanged. This finding is consistent with previous predictions, thus the average values can be taken for A and r.

4.2.3. Ordinate B of the impedance circle center. Equation (16) should be solved numerically to determine ordinate B. Because the smallest adjustable amount of the compensation capacitance used in the experiment is 1 nF, it can be seen from figure 8 that the zero compensation capacitance C_0 is
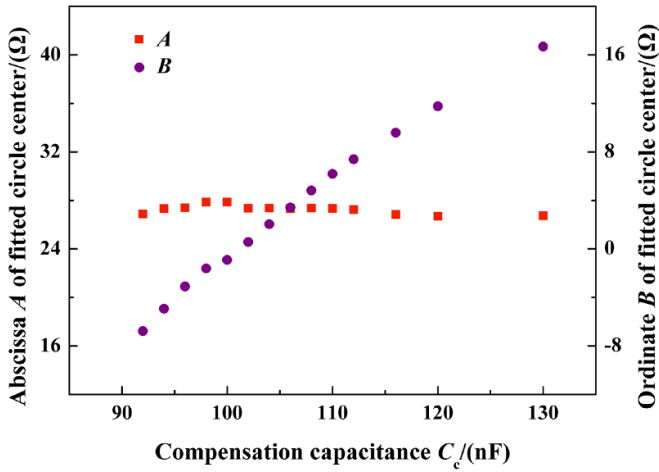
Figure 8. Relationship between the abscissa *A* and ordinate *B* of the fitted circle center and the compensation capacitance C_c of the GMUT.
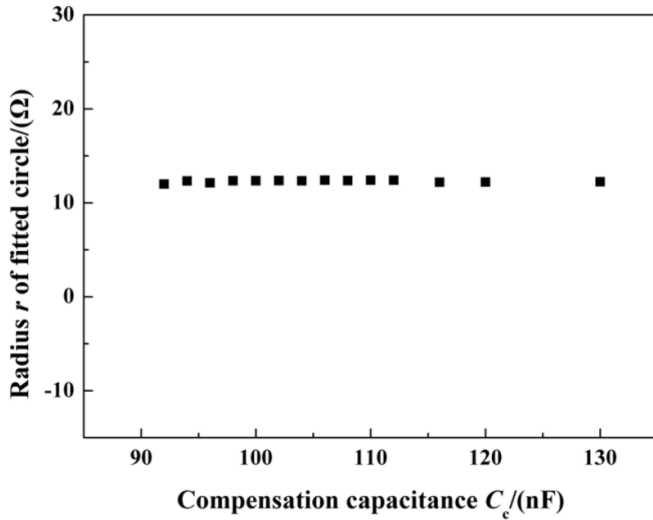
Figure 9. Relationship between the radius *r* of the fitted circle and the compensation capacitance C_c of the GMUT.

between 98 nF-104 nF. Nonlinear curve fitting was carried out in OriginPro 8, and zero compensation capacitance between 98 nF and 104 nF was selected for respective fitting. Thus, the identified parameters C_0 and $\overline{\omega}$ for the minimum nonlinear fitting error for B can be derived in figure 10.

4.2.4. Improved model validation.　　To verify the effectiveness of the improved impedance-compensation model, the assumptions must be verified. For the effective cut-off frequency interval $[\overline{f_1}, \overline{f_2}]$, by substituting the identified parameter C_0 and the mechanical resonance circular frequency ω_n into equation (10), the L_e can be then calculated as:

$$L_e = \frac{1}{\omega_n^2 C_0}. \quad (26)$$
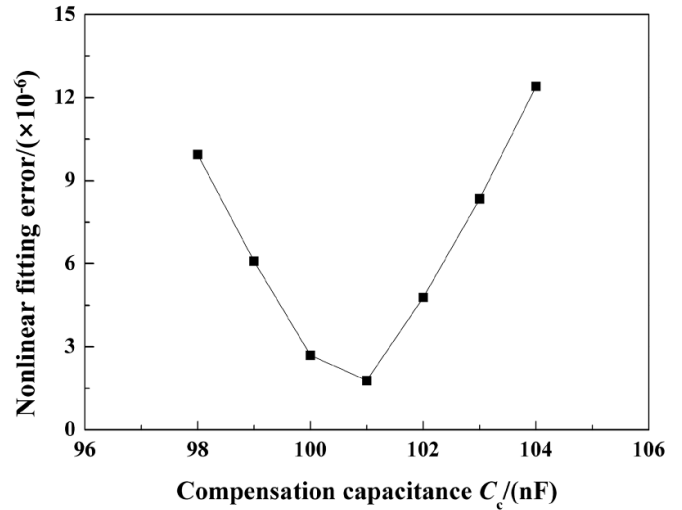
Figure 10. Nonlinear fitting error of the ordinate *B* of the impedance circle center under different compensation capacitances.

By substituting equations (13) and (26) into equation (8), *B* can be rewritten as equation (27):

$$B = 2\pi f L_e - \frac{1}{2\pi f C_c} = \frac{2\pi f}{\omega_n^2 C_0} - \frac{1}{2\pi f C_c} = \frac{f}{2\pi f_n^2 C_0} - \frac{1}{2\pi f C_c}. \quad (27)$$

Therefore, when *f* is in the interval $[\overline{f_1}, \overline{f_2}]$, the changed value ΔB for $C_c = C_0$ can be calculated according to equation (27), i.e. $\Delta B= 0.84$ Ω, and the average experimental changed value $\overline{\Delta B}$ for a variety of compensation capacitances is just 0.83 Ω. The findings show that the assumption of ignoring the frequency change within the effective cut-off frequency interval is reasonable, relative to the total impedance mode.

In this case, to validate the ordinate *B*, the mathematical model of the coordinate *B* in equation (16) can be established according to the identified parameters C_0 and $\overline{\omega}$ in figure 10. The fitting results for the coordinate *B* are shown in figure 11, and the data fitting effect is good, which means the assumption of the mathematical model of *B* is reasonable.

Substituting the identified parameters *A, B,* and *r* into equation (9), the improved impedance-compensation model of the GMUT is obtained:

$$(R - 27.25)^2 + [X - 7409.11(\frac{1}{101} - \frac{1}{C_c})]^2 = 12.30^2. \quad (28)$$

To verify the validity of the improved impedance-compensation model of the GMUT, validation of the improved impedance-compensation model is shown in figure 12. As illustrated in the figure, the model has a good fitting result with the points used for fitting in figure 12(a). To better distinguish the fitting effect for varied compensation capacitances, a comparison of the fitting results and the impedance circles under five kinds of compensation capacitances with large differences is provided in figure 12(b), illustrating that the improved impedance-compensation model of the GMUT corresponds well with the experimental results.
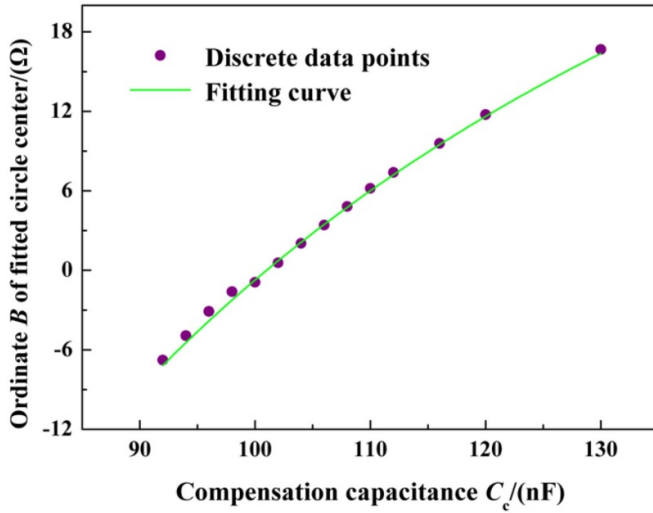
Figure 11. Comparison of the discrete data points and the fitting curve of the ordinate *B* of the impedance circle center under different compensation capacitances.

4.3. Impedance-compensation method for determining the maximum amplitude

4.3.1. Relationship between the frequency and frequency angle of the impedance circle.
The relation curve between the frequency f and the frequency angle α of the impedance circle in a certain experimental range of the compensation capacitance is provided in figure 13. In the figure, (a), (b), (c), and (d) respectively represent the first, second, third, and fourth intervals in figure 3. It can be seen from figure 13 that the curves under different compensation capacitances obey the same rule and the frequency change of the discrete data points in (a), (c), and (d) is far smaller than that in (b). It should be noted that the discrete data points at the beginning of the frequency-sweeping experiment in (b) and (c) were removed as they were not in use.

4.3.2. Extreme frequency difference model.
The resonance frequency will be affected by the excitation signal [21]. Therefore, in order to more effectively explore the method for determining the maximum amplitude, the extreme frequency difference model is proposed to illustrate the frequency variation between the minimum current and the maximum current in the impedance circle. The curves in (a) and (d) and the curves in (b) and (c) in figure 13 are established under the same abscissa α_{ext} according to equation (19), as shown in figure 14.

In figure 14, the f-α_{ext} curves under different compensation capacitances have the same change trend. The curves can thus be fitted by the least square method and the corresponding mathematical model can be established. To facilitate calculation, one group of data ($C_c = 100$ nF) was selected as the discrete data points for fitting, and the polynomial nonlinear fitting according to the least square method was performed in Stata/SE 14.0. The R-squared of the fitting functions $f_{14}(\alpha)$ and $f_{23}(\alpha)$, which are respectively applicable to the curves in

Table 2. Polynomial fitting coefficient.

Item	Subscript 14	Subscript 23
a	-7.67205×10^{-10}	-2.97931×10^{-11}
b	-5.55275×10^{-8}	6.91323×10^{-9}
c	-3.10338×10^{-6}	-5.67383×10^{-7}
d	-4.98215×10^{-4}	2.09382×10^{-5}
e	-1.91811×10^{-1}	-6.24385×10^{-4}
f	2.07035×10^{4}	3.59366×10^{-2}
g	-	-1.81493×10^{0}
h	-	2.07717×10^{4}

(a) and (d) and the curves in (b) and (c), reaches saturation at $i = 5$ and $i = 7$, respectively. Therefore, the fitting functions of the model are established by selecting the corresponding polynomial orders, as shown in equation (29):

$$\begin{cases} f_{14}(\alpha) = a_{14}\alpha^5 + b_{14}\alpha^4 + c_{14}\alpha^3 + d_{14}\alpha^2 + e_{14}\alpha + f_{14} \\ f_{23}(\alpha) = a_{23}\alpha^7 + b_{23}\alpha^6 + c_{23}\alpha^5 + d_{23}\alpha^4 + e_{23}\alpha^3 \\ \qquad + f_{23}\alpha^2 \end{cases}$$
(29)

where the fitting results are expressed by scientific counting method with six significant figures reserved, as shown in table 2. The fitting curves are expressed in figure 14.

In figure 14, Δf_{p-p} represents the extreme frequency difference between the extreme frequency for the minimum current and the extreme frequency for the maximum current obtained in the impedance circle. Therefore, according to the fitting functions of the model $f_{14}(\alpha)$ and $f_{23}(\alpha)$, the extreme frequency difference model of the impedance circle can be established, as shown in equation (30):

$$\Delta f_{p-p}(\alpha_{ext}) = f_{23}(\alpha_{ext}) - f_{14}(\alpha_{ext})$$
(30)

where, $\Delta f_{p-p}(\alpha_{ext})$ refers to the extreme frequency difference of the extreme frequency angle α_{ext}. For the GMUT with different compensation capacitances, different excitation voltages were used for the frequency-sweeping experiment, with 10 Hz as the frequency step. The comparison of the experimental result of the extreme frequency difference Δf_{p-p} and the predicted result under different compensation capacitances is shown in figure 15.

In figure 15, as the increase of α_{ext}, Δf_{p-p} and the variation amplitude of Δf_{p-p} both decrease gradually, the extreme frequency difference meets the predicted result given by equation (30) under different excitation voltages and compensation capacitances. This finding illustrates that the GMUT under different compensation capacitances and excitation voltages follows the same rule for the extreme frequency difference between the minimum current and the maximum current, which can be useful to determine the actual resonance frequency of the GMUT.

4.3.3. Impedance-compensation characteristics.
To explorethe impedance-compensation characteristics, the frequencies corresponding to the extreme frequency angles and the resistance frequency angles must be studied. Considering
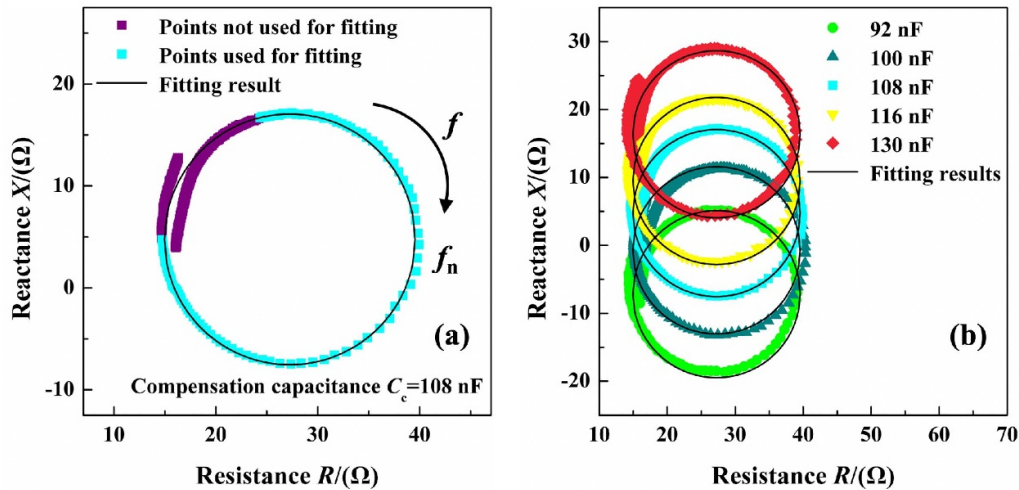
Figure 12. Validation of the improved impedance-compensation model of the GMUT: (a) Fitting result with points used and not used for fitting; (b) Model validation.
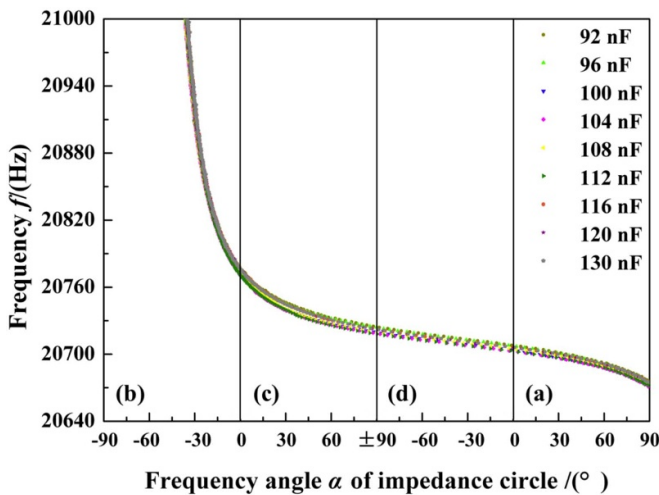
Figure 13. Relationship between the frequency f and the frequency angle α of the impedance circle under different compensation capacitances: (a), (b), (c) and (d) respectively represent the first, second, third, and fourth intervals in .figure 3
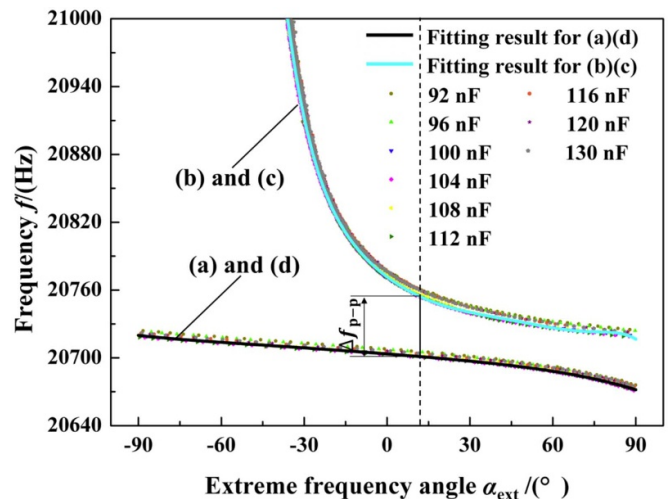
Figure 14. Relationship between the frequency f and the extreme frequency angle α_{ext} of the impedance circle under different compensation capacitances.

the characteristics of the extreme frequency difference model in figure 15, the frequency difference between the maximum current and minimum current increases rapidly when $C_c < C_0 = 101$ nF. Since the frequency of the minimum current is near the mechanical resonance frequency f_n, relatively insensitive to the compensation capacitances as shown in figure 16, the frequency of the high current is more likely to deviate from the mechanical resonance frequency f_n than $C_c \geq C_0$. Thus, $C_c \geq C_0$ was selected for the resonance frequency.

Substituting the identified parameters into equation (23), when $\alpha_{\text{res1}}(C_c) = -90°$, $C_c \approx 121$ nF was obtained. Therefore, 101 nF $\leq C_c \leq 121$ nF was selected to illustrate the impedance-compensation characteristics including the extreme currents and the resistance points. The Relationship between the fitting results of the resistance frequencies

and extreme frequencies and the resistance frequency angle α_{res1} is shown in figure 16, in which f_{res1} and f_{res2} represent the frequencies corresponding to the resistance frequency angles α_{res1} and α_{res2} of the impedance circle, with the same phases of the voltage and current. Additionally, f_{ext1} and f_{ext2} represent the frequencies corresponding to the extreme frequency angles α_{ext1} and α_{ext2} of the impedance circle, with the corresponding minimum and maximum currents, respectively. All the above frequencies were obtained according to equations (21), (24), (29), and table 2.

In figure 16, as the compensation capacitance C_c increases, α_{res1} decreases from $0°$ to $-90°$, the extreme frequency difference between the minimum current and the maximum current in the impedance circle decreases, and the resistance frequency difference between the two in-phase points of the current
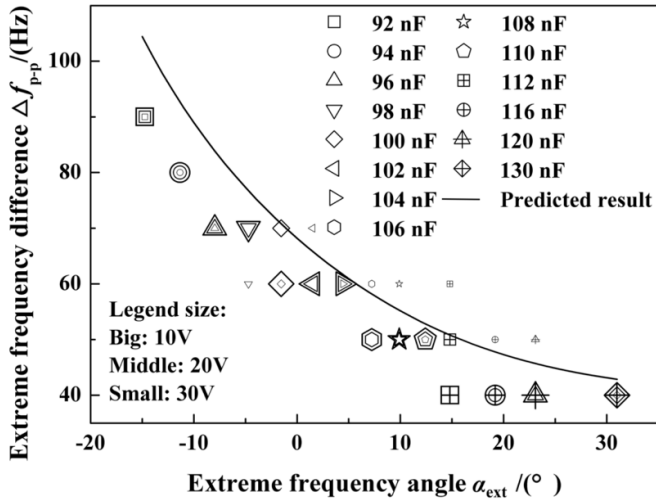
Figure 15. Comparison of the experimental result of the extreme frequency difference Δf_{p-p} and the predicted result under different compensation capacitances.
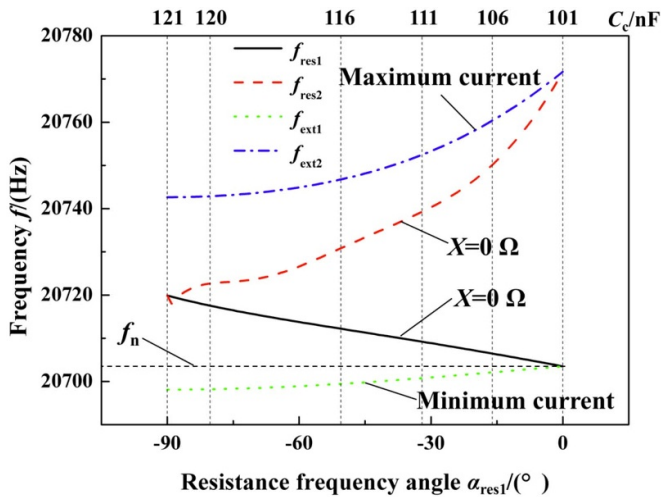
Figure 16. Relationship between the fitting results of the resistance frequencies and extreme frequencies and the resistance frequency angle α_{res1}.

and voltage in the impedance circle converges to the same frequency.

4.3.4. Maximum amplitude and actual resonance frequency.

The above research illustrates that when the compensation capacitance is equal to zero compensation capacitance ($C_c = C_0$), the minimum current and maximum current in the impedance circle are resistive. However, due to the characteristics of the extreme frequency, the current increases as the frequency is far away from the mechanical resonance frequency f_n of the GMUT. Because the mechanical resonance frequency f_n is relatively large, when the frequency is in the effective range of $f_n \pm \Delta f$, where Δf is a frequency offset, it is still considered as the mechanical resonance state. As the excitation frequency $f < f_n$, the discrete data points are more densely distributed than $f > f_n$, which means the frequency is easier
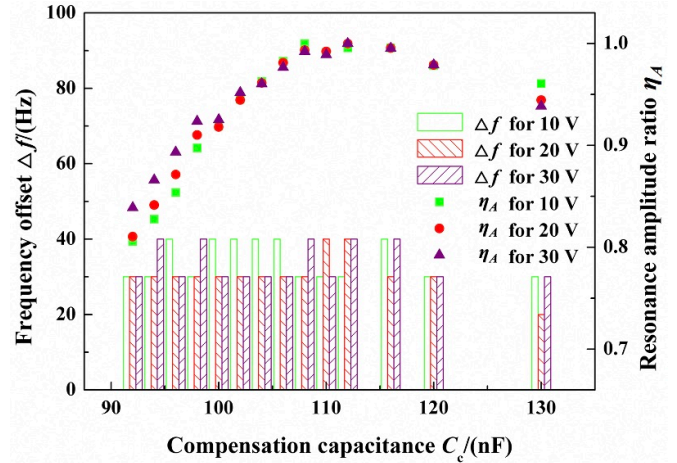
Figure 17. Relationship between the frequency offset Δf and resonance amplitude ratio η_A and the compensation capacitance C_c of the GMUT.

to deviate from the mechanical resonance frequency f_n. Thus, the resonance frequency was studied in $f > f_n$ (i.e. $f_n + \Delta f$). It can be seen from figure 16 that the greater the frequency deviating from the mechanical resonance frequency f_n, the closer the current is to the maximum current.

The vibration frequency of the system is consistent with the excitation frequency of the input electrical signal, and different excitation frequencies lead to different input energy due to the impedance characteristics of the GMUT. When the voltage and current are at the same phase (electrical resonance), the input energy will all be converted into useful work. Therefore, when the GMUT is excited in the effective range of the mechanical resonance state, the actual resonance frequency will occur at the frequency with maximum useful work (generally near electrical resonance). Thus, the maximum amplitude related to the optimum resonance may occur at the optimal point where the mechanical resonance and electrical resonance occur nearly simultaneously.

Because the extreme frequency difference model is independent of the excitation voltage, it is, therefore, applicable to determine the actual resonance frequency for the maximum amplitude using the extreme frequency difference model, regardless of the influence of the excitation signal on the resonance frequency. As compensation capacitance increases, the frequencies of the two resistance points gradually approach, the distribution for the frequencies with highly identical phase of the voltage and current between the extreme frequencies of the minimum current and maximum current is more uniform. Therefore, there may be an optimal compensation capacitance range in producing a maximum amplitude. It is thus supposed that the actual resonance frequency of the maximum amplitude can be obtained at the frequency of the minimum current plus the frequency offset Δf. To verify the above hypothesis, the resonance amplitude ratio η_A is defined as:

$$\eta_A = \frac{A}{A_{\max}} \tag{31}$$

where *A* represents the resonance amplitude of each compensation capacitance at the same excitation voltage and A_{max} (i.e. the maximum amplitude) is the maximum *A* in the experiments at each excitation voltage, as shown in figure 17.

In figure 17, the resonance amplitude ratio η_A reaches the maximum value in the optimal compensation capacitance range and the frequency offset Δf is almost 30 Hz for each compensation capacitance and each excitation voltage. Taking the Δf into figure 16, it can be found that the electrical resonance almost occurs in the optimal compensation capacitance range, that is to say, although the energy conversion efficiency does not reach the maximum (close to the maximum), the maximum amplitude is generated due to the maximum useful work input to the GMUT. Thus the method for determining the maximum amplitude and the actual resonance frequency used as the frequency tracking index at each excitation voltage can be obtained.

5. Conclusions

Investigation on the optimum resonance of the giant magnetostrictive ultrasonic transducer (GMUT) with capacitance-based impedance compensation was conducted in this work. The results show that the improved impedance-compensation model is in good agreement with the impedance circle of the GMUT, and the following conclusions can be drawn.

(1) Under different excitation voltages and compensation capacitances, the extreme frequency difference between the minimum current and maximum current meets the predicted model, which is not affected by excitation voltage and the compensation capacitance.

(2) As the compensation capacitance increases from zero compensation capacitance, the resistance frequency difference between the two in-phase points of the current and voltage in the impedance circle of the GMUT converges to the same frequency.

(3) The method for determining the maximum amplitude related to the optimum resonance of the GMUT is illustrated to be effective. The actual resonance frequency used as the frequency tracking index under different excitation voltages and compensation capacitances can be obtained at the frequency of the minimum current plus a frequency offset.

Acknowledgments

Conflict of interest

The authors declare that they have no conflict of interest to report.

ORCID iDs

Huilin Zhou ⓘ https://orcid.org/0000-0003-1003-2527
Jianfu Zhang ⓘ https://orcid.org/0000-0002-7672-7682

References

[1] Verma G C, Pandey P M and Dixit U S 2018 Modeling of static machining force in axial ultrasonic-vibration assisted milling considering acoustic softening *Int. J. Mech. Sci.* **136** 1–16

[2] Geng D, Liu Y, Shao Z, Lu Z, Cai J, Li X, Jiang X and Zhang D 2019 Delamination formation, evaluation and suppression during drilling of composite laminates: a review *Compos. Struct.*

[3] Wang H, Pei Z and Cong W 2020 A feeding-directional cutting force model for end surface grinding of CFRP composites using rotary ultrasonic machining with elliptical ultrasonic vibration *Int. J. Mach. Tools Manuf.* 103540

[4] Sun X, Liu Y, Hu W, Sun T and Hu J 2020 Design optimization of a giant magnetostrictive driving system for large stroke application considering vibration suppression in working process *Mech Syst Signal Process* **138** 106560

[5] Youssef G, Nacy S and Newacheck S 2020 Dynamic magnetoelectric response of composite multiferroics cylinders *Smart Mater. Struct.* **29** 035025

[6] Vjuginova A A, Durukan Y and Novik A A 2020 Excitation of large axisymmetric bodies by magnetostrictive ultrasonic transducers. *2020 IEEE Conf. of Russian Young Researchers in Electrical and Electronic Engineering (EIConRus)* IEEE

[7] Zhou H, Zhang J, Feng P, Yu D and Wu Z 2019 Design on amplitude prediction model for a giant magnetostrictive ultrasonic transducer *Ultrasonics* 106017

[8] Zhou H, Zhang J, Feng P, Yu D, Cai W and Wang J 2020 Performance evaluation of a giant magnetostrictive rotary ultrasonic machine tool *Int. J. Adv. Manuf. Technol.* **106** 3759–73

[9] Jin K, Kou Y and Zheng X 2012 The resonance frequency shift characteristic of Terfenol-D rods for magnetostrictive actuators *Smart Mater. Struct.* **21** 045020

[10] Hou H, Finkel P, Staruch M, Cui J and Takeuchi I 2018 Ultra-low-field magneto-elastocaloric cooling in a multiferroic composite device *Nat. Commun.* **9** 1–8

[11] Yang Y, Yang B and Niu M 2018 Adaptive trajectory tracking of magnetostrictive actuator based on preliminary hysteresis compensation and further adaptive filter controller *Nonlinear Dyn.* **92** 1109–18

[12] Zeng H and Zeng G 2012 Nonlinear behaviors of giant magnetostrictive high power ultrasonic transducer *Appl. Mech. Mater.* **128-129** 918–22

[13] Zhou C, Duan J-A, Deng G and Li J 2017 Improved thermal characteristics of a novel magnetostrictive jet dispenser using water-cooling approach *Appl. Therm. Eng.* **112** 1–6

[14] Cai W, Feng P, Zhang J, Wu Z and Yu D 2016 Effect of temperature on the performance of a giant magnetostrictive ultrasonic transducer *J. Vibroeng.* **18** 1307–18

[15] Zhang H, Wang F, Zhang D, Hou Y and Xi T 2015 A new automatic resonance frequency tracking method for piezoelectric ultrasonic transducers used in thermosonic wire bonding *Sensors Actuators* A **235** 140–50

[16] Yang M, Li S-Y, Zhuang X-Q, Yang T-Y and Zhou M. 2016 An improved frequency tracking strategy in ultrasonic

transducer. *2016 Symp. on Piezoelectricity, Acoustic Waves, and Device Applications (SPAWDA)* IEEE

[17] Xu A 2009 Method of automatic following resonance frequency for giant magnetostrictive transducer *Proc. CSEE* **25** 114–8

[18] Cai W, Zhang J, Feng P, Yu D and Wu Z 2017 A bilateral capacitance compensation method for giant magnetostriction ultrasonic processing system *Int. J. Adv. Manuf. Technol.* **90** 2925–33

[19] Calkins F T 1997 Design, analysis, and modeling of giant magnetostrictuve transducers Ph.D. Dissertation Aerospace Engineering-Iowa State University

[20] Hall D L 1994 Dynamics and vibrations of magnetostrictive transducers Ph.D. Dissertation Aerospace Engineering-Iowa State University

[21] Cai W, Zhang J, Yu D, Feng P and Wang J 2018 A vibration amplitude model for the giant magnetostrictive ultrasonic processing system *J. Intell. Mater. Syst. Struct.* **29** 574–84